J|A|C|S
ARTICLES
Published on Web 06/17/2002

Electron-Mediating Cu_A Centers in Proteins: A Comparative High Field ^1H ENDOR Study

Boris Epel,[†] Claire S. Slutter,[†] Frank Neese,[§,○] Peter M. H. Kroneck,[§] Walter G. Zumft,[||] Israel Pecht,[‡] Ole Farver,[⊥] Yi Lu,[#] and Daniella Goldfarb*[,†]

Contribution from the Departments of Chemical Physics and Immunology, Weizmann Institute of Science, Rehovot, Israel, Faculty of Biology, University of Konstanz, D-78457 Konstanz, Germany, Lehrstuhl für Mikrobiology, Universität Fridericiana, D-76128 Karlsruhe, Germany, Royal Danish School of Pharmacy, Institute of Analytical & Pharmaceutical Chemistry, DK-2100 Copenhagen, Denmark, and Department of Chemistry, University of Illinois, Urbana, Illinois 61801

Received November 9, 2001. Revised Manuscript Received March 4, 2002

Abstract: High field (W-band, 95 GHz) pulsed electron-nuclear double resonance (ENDOR) measurements were carried out on a number of proteins that contain the mixed-valence, binuclear electron-mediating Cu_A center. These include nitrous oxide reductase (N_2OR), the recombinant water-soluble fragment of subunit II of *Thermus thermophilus* cytochrome *c* oxidase (COX) ba_3 (M160T9), its M160QT0 mutant, where the weak axial methionine ligand has been replaced by a glutamine, and the engineered "purple" azurin (purpAz). The three-dimensional (3-D) structures of these proteins, apart from the mutant, are known. The EPR spectra of all samples showed the presence of a mononuclear Cu(II) impurity with EPR characteristics of a type II copper. At W-band, the $g_\perp$ features of this center and of Cu_A are well resolved, thus allowing us to obtain a clean Cu_A ENDOR spectrum. The latter consists of two types of ENDOR signals. The first includes the signals of the four strongly coupled cysteine β-protons, with isotropic hyperfine couplings, A_{iso}, in the 7−15 MHz range. The second group consists of weakly coupled protons with a primarily anisotropic character with $A_{zz} < 3$ MHz. Orientation selective ENDOR spectra were collected for N_2OR, M160QT0, and purpAz, and simulations of the cysteine β-protons signals provided their isotropic and anisotropic hyperfine interactions. A linear correlation with a negative slope was found between the maximum A_{iso} value of the β-protons and the copper hyperfine interaction. Comparison of the best-fit anisotropic hyperfine parameters with those calculated from dipolar interactions extracted from the available 3-D structures sets limit to the sulfur spin densities. Similarly, the small coupling spectral region was simulated on the basis of the 3-D structures and compared with the experimental spectra. It was found that the width of the powder patterns of the weakly coupled protons recorded at $g_\perp$ is mainly determined by the histidine $H_{\epsilon 1}$ protons. Furthermore, the splitting in the outer wings of these powder patterns indicates differences in the positions of the imidazole rings relative to the Cu_2S_2 core. Comparison of the spectral features of the weakly coupled protons of M160QT0 with those of the other investigated proteins shows that they are very similar to those of purpAz, where the Cu_A center is the most symmetric, but the copper spin density and the $H_{\epsilon 1}$−Cu distances are somewhat smaller. All proteins show the presence of a proton with a significantly negative A_{iso} value which is assigned to an amide proton of one of the cysteines. The simulations of both strongly and weakly coupled protons, along with the known copper hyperfine couplings, were used to estimate and compare the spin density distribution in the various Cu_A centers. The largest sulfur spin density was found in M160T9, and the lowest was found in purpAz. In addition, using the relation between the A_{iso} values of the four cysteine β-protons and the H−C−S−S dihedral angles, the relative contribution of the hyperconjugation mechanism to A_{iso} was determined. The largest contribution was found for M160T9, and the lowest was found for purpAz. Possible correlations between the spin density distribution, structural features, and electron-transfer functionality are finally suggested.

Introduction

Two types of copper centers in proteins are known to mediate electron transfer (ET): the abundant type I (T1), which is a mononuclear copper binding site, and the mixed-valence binuclear Cu_A center.[1] T1 sites are present, for example, in azurin and pseudoazurin, which are electron carriers in bacterial energy conversion systems,[2] and in plastocyanin, which mediates electrons between cytochrome b_6f complex and photosystem I.[3] It is also found in blue-copper oxidases such as laccase, ascorbate oxidase, and ceruloplasmin, and in the copper nitrite

* To whom correspondence should be addressed. E-mail: daniella.goldfarb@weizmann.ac.il.
[†] Department of Chemical Physics, Weizmann Institute of Science.
[‡] Department of Immunology, Weizmann Institute of Science.
[§] University of Konstanz.
[||] Universität Fridericiana.
[⊥] Royal Danish School of Pharmacy.
[#] University of Illinois.
[○] Current address: Max-Planck Institut für Strahlenchemie, Stiftstrasse 34-36, D-45470 Mülheim an der Ruhr, Germany.

(1) *Handbook of Metalloproteins*; Messerschmidt, A., Huber, R., Poulos, T., Wieghart, K., Eds.; John Wiley and Sons: New York, 2001; Vol. 2, pp 1149−1345.
(2) Kolczac, U.; Dennison, C.; Messerschmidt, A.; Canters, G. W. In *Handbook of Metalloproteins*; Messerschmidt, A., Huber, R., Poulos, T., Wieghart, K., Eds.; John Wiley and Sons: New York, 2001; Vol. 2, pp 1170−1194.
(3) Freeman, H. C.; Guss, J. M. *Handbook of Metalloproteins*; John Wiley and Sons: New York, 2001; Vol. 2, pp 1153−1169.

10.1021/ja012514j CCC: $22.00

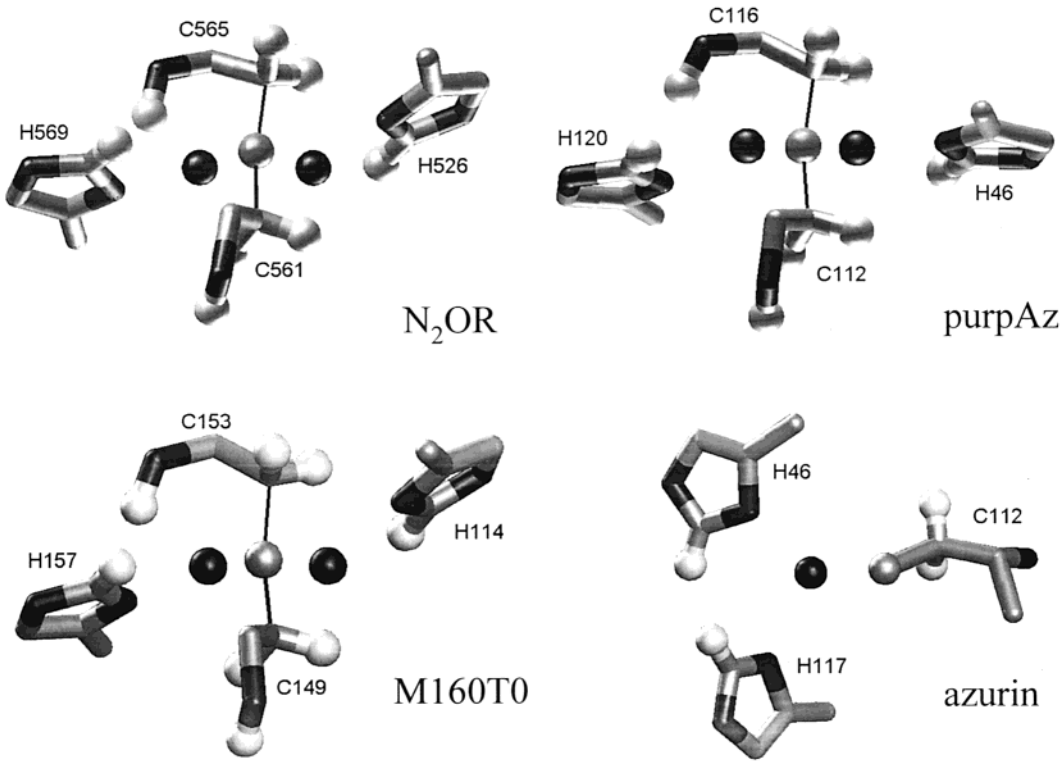

Figure 1. The 3-D structures of the nearest ligands of Cu_A sites in N_2OR (2.4 Å resolution),[20] M160T0 (1.6 Å resolution),[21] and purpAz (1.65 Å resolution)[12] from a projection along the S−S direction of the Cu_2S_2 core, as compared to that of T1 of azurin.[15] Black, gray, and white spheres represent atoms of Cu, S, and H, accordingly.

reductases, in all of which it serves as the initial electron-accepting site.[4] While the structure of the T1 site has been known for a long time (the 3-D structure of plastocyanin has been determined already in 1977[5]), Cu_A has been recognized as a binuclear center much later.[6,7] It is the initial electron acceptor in cytochrome *c* oxidase (COX) and in nitrous oxide reductase (N_2OR).[8] In addition, the quinol oxidase subunit II (CyoA)[9] and azurin (purple azurin, purpAz)[10,12] were converted by mutagenesis to form Cu_A centers. A recombinant water-soluble fragment of subunit II of *Thermus thermophilus* COX ba_3 that contains the Cu_A site has been prepared (M160T0) as well.[13] The 3-D structures of all of these proteins have been determined by X-ray crystallography.[9,12,14−18,20,21] Figure 1 shows the T1 copper site of azurin[15] together with the Cu_A centers in M160T0,[21] N_2OR,[20] and purpAz.[12] The copper ion in T1 is coordinated to a cysteine thiolate and two imidazole residues of histidine in a trigonal arrangement with rather short bonds (∼2 Å) and a fourth, weaker axial ligand (usually a thioether of methionine) at a distance of ∼3 Å.[14,15,22,23] The Cu_A center resembles two fused T1 centers, with thiolates of two cysteines, two histidine imidazoles, and two weak axial ligands, a methionine sulfur, and a main chain carbonyl oxygen of glutamine.[9,12,14−21]

Considerable efforts have focused on studying the relation between the 3-D structure of the Cu_A site, its spectroscopic properties, and electronic structure and ET characteristics such as redox potentials and reorganization energies.[24−26] The unusual

(4) Messerschmidt, A. In *Handbook of Metalloproteins*; Messerschmidt, A., Huber, R., Poulos, T., Wieghart, K., Eds.; John Wiley and Sons: New York, 2001; Vol. 2, pp 1345−1358. Davies, G. D.; Ducros, V. In *Handbook of Metalloproteins*; Messerschmidt, A., Huber, R., Poulos, T., Wieghart, K., Eds.; John Wiley and Sons: New York, 2001; Vol. 2, pp 1359−1368. Lindley, P. F. In *Handbook of Metalloproteins*; Messerschmidt, A., Huber, R., Poulos, T., Wieghart, K., Eds.; John Wiley and Sons: New York, 2001; Vol. 2, pp 1369−1380. Adman, E. T.; Murphy, M. E. P. In *Handbook of Metalloproteins*; Messerschmidt, A., Huber, R., Poulos, T., Wieghart, K., Eds.; John Wiley and Sons: New York, 2001; Vol. 2, pp 1381−1390.
(5) Chapman, G. V.; Colman, P. M.; Freeman, H. C.; Guss, J. M.; Murata, M.; Norris, V. A.; Ramshaw, J. A. M.; Venkatappa , M. P. *J. Mol. Biol.* **1977**, *110*, 187−189.
(6) Kroneck, P. M. H.; Antholine, W. E.; Riester, J.; Zumft, W. G. *FEBS Lett.* **1989**, *248*, 212−213.
(7) Antholine, W. E.; Kastrau, D. H. W.; Steffens, G. C. M.; Buse, G.; Zumft, W. G., Kroneck, P. M. H. *Eur. J. Biochem.* **1992**, *209*, 875−891.
(8) Kroneck, P. M. H. In *Handbook of Metalloproteins*; Messerschmidt, A., Huber, R., Poulos, T., Wieghart, K., Eds.; John Wiley and Sons: New York, 2001; Vol. 2, pp 1333−1341.
(9) Wilmanns, M.; Lappalainen, P.; Kelley, M.; Sauer-Eriksson, E.; Saraste, M. *Proc. Natl. Acad. Sci. U.S.A.* **1995**, *92*, 11955−11959.
(10) Hay, M.; Richards, J. H.; Lu, Y. *Proc. Natl. Acad. Sci. U.S.A.* **1996**, *93*, 461−464.
(11) Hay, M.; Ang, M.; Gamelin, D. R.; Solomon, E. I.; Antholine, W. E.; Ratle, M.; Blackburn, N. J.; Massey, P. D.; Wang, X.; Kwon, A. H.; Lu, Y. *Inorg. Chem.* **1998**, *37*, 191−198.
(12) Robinson, H.; Ang, M. C.; Gao, Y. G.; Hay, M. T.; Lu, Y.; Wang, A. H. J. *Biochemistry* **1999**, *38*, 5677−5683.
(13) Slutter, C. E.; Sanders, D.; Wittung, P.; Malmström, B. G.; Aasa, R.; Richards, J. H.; Gray, H. B.; Fee, J. A. *Biochemistry* **1996**, *35*, 3387−3395.
(14) Baker, E. N. *J. Mol. Biol.* **1988**, *203*, 1071−1095.
(15) Nar, H.; Messerschmidt, A.; Huber, R.; van de Kamp, M.; Canters, G. W. *J. Mol. Biol.* **1991**, *221*, 765−772.
(16) Iwata, S.; Ostermeier, C.; Ludwig, B.; Michel, H. *Nature* **1995**, *376*, 660−669.
(17) Tsukihara, T.; Aoyama, H.; Yamashita, E.; Tomizaki, T.; Yamaguchi, H.; Shinzawa-Itoh, K.; Nakashima, R.; Yaono, R.; Yoshikawa, S. *Science* **1995**, *269*, 1069−1074.
(18) Tsukihara, T.; Aoyama, H.; Yamashita, E.; Tomizaki, T.; Yamaguchi, H.; Shinzawa-Itoh, K.; Nakashima, R.; Yaono, R.; Yoshikawa, S. *Science* **1996**, *272*, 1136−1144.
(19) Yoshikawa, S.; Shinzawa-Itoh, K.; Nakashima, R.; Yaono, R.; Yamashita, E.; Inoue, N.; Yao, M.; Fei, M. J.; Libeu, C. P.; Mizushima, T.; Yamaguchi, H.; Tomizaki, T.; Tsukihara, T. *Science* **1998**, *280*, 1723−1729.
(20) Brown, K.; Tegoni, M.; Prudêncio, M.; Pereira, A. S.; Besson, S.; Moura, J. J.; Moura, I.; Cambillau, C. *Nat. Struct. Biol.* **2000**, *7*, 191−195.
(21) Williams, P. A.; Blackburn, N. J.; Sanders, D.; Bellamy, H.; Stura, E. A.; Fee, J. A.; McRee, D. E. *Nat. Struct. Biol.* **1999**, *6*, 509−516.
(22) Messerschmidt, A.; Ladenstein, R.; Huber, R.; Bolognesi, M.; Avigliano, L.; Petruzzelli, R.; Rossi, A.; Finazzi-Agro, A. *J. Mol. Biol.* **1992**, *224*, 179−205.
(23) Guss, J. M.; Freeman, H. C. *J. Mol. Biol.* **1983**, *169*, 521−563.

spectroscopic properties, the strong blue color of T1 and the dark purple color of Cu_A, stem from the S−Cu charge-transfer bands. The ^{63,65}Cu hyperfine interaction of T1 is unusually small[27,28] because of the highly covalent nature of the Cu−S coordination and the large spin density on the sulfur. The Cu_A center in the resting state has a total of one unpaired electron which is highly delocalized, with each copper having a formal oxidation state of 1.5.[8] The ^{63,65}Cu hyperfine coupling is in this case about one-half that of the T1 Cu(II) because of the delocalization of the unpaired electron over the two coppers.[6] The highly covalent Cu−S bonds in both T1 and Cu_A were found to be important for coupling into the ET pathways.[25,29]

One of the spectroscopic techniques that is most commonly used for the characterization of these ET-mediating centers is EPR spectroscopy. It provided the *g*- and ^{63,65}Cu hyperfine interactions that characterize the ground state and the spin delocalization. In addition, the EPR related methods, electron-nuclear double resonance (ENDOR)[30−34] and electron-spin-echo envelope modulation (ESEEM)[35−37] spectroscopies, have played an important role in the identification of the ligands constituting the coordination sphere of the copper ions and the spin delocalization over the site. X-band ESEEM spectroscopy has been most useful in the determination of the hyperfine and quadrupole couplings of weakly coupled ^{14}N nuclei such as the remote nitrogens of the histidines' imidazole and main chain amides.[36,38,39] The more strongly coupled nuclei, the cysteine β-protons and the directly bound histidine nitrogens, have been examined by X-band ENDOR.[31,34] It has been shown that the weakly coupled nitrogens of azurin can also be detected by ENDOR at high fields in single crystals.[40]

The isotropic hyperfine coupling of the cysteine β-protons is an important source of structural information because it depends on the H−C−S−Cu dihedral angle in T1[41] and the H−C−S−S dihedral angle in Cu_A.[31,42] Similarly, the hyperfine coupling of the histidine protons, specifically of the $H_{\epsilon 1}$ protons, can provide spin density and structural information. Moreover, the availability of experimental values of hyperfine interactions of ligand nuclei, which characterize the highly delocalized nature of the unpaired electron wave function, serves as important experimental constraints for the determination of the ground state by quantum chemical calculations.[26,43] This may then provide the rationale for the unique properties of these ET sites.[25] Unfortunately, the ENDOR spectra of T1 and Cu_A centers recorded at X-band frequencies often suffer from low resolution because of overlap of ^{1}H signals with those of the directly bound ^{14}N.[31,41] This problem can be alleviated by recording the spectra at Q-band,[34,41] but the reported ^{1}H spectra are often distorted and show only the high-frequency part of the symmetric ENDOR spectrum. Another problem of X-band ENDOR and ESEEM studies of the Cu_A center is interferences from signals of a mononuclear Cu(II) impurity center.[44]

We have now employed high field (95 GHz) ^{1}H ENDOR spectroscopy in a comparative study of the Cu_A site present in four different proteins: N_2OR, the soluble fragment of COX, M160T9, which is nine amino acids shorter than the original M160T0, the M160QT0 mutant, and purpAz. The spectra are free of ^{14}N signals, well resolved, symmetric, and not distorted. Moreover, problems caused by contribution from mononuclear Cu(II), present in some of the proteins, were eliminated by the separation of the $g_\perp$ singularities of Cu_A and T2. The larger spread of the EPR powder pattern also leads to better orientation selection that allows a more accurate determination of the isotropic and anisotropic hyperfine components. The study of several different Cu_A sites allowed us to compare their sulfur and copper spin densities. This, combined with the available 3-D structures, permitted us to suggest some correlations between the hyperfine parameters of weakly and strongly coupled protons, the spin density distribution, and structural properties of these sites.

Experimental Section

Sample Preparations. Azurin from *Pseudomonas aeruginosa* was obtained as described.[37] The sample concentration was 2 mM in a 100 mM Hepes buffer pH = 7. M160T0 is a product of the original soluble fragment construct of cytochrome ba_3 from *Thermus thermophilus* that encodes 135 amino acids of subunit II, omitting the transmembrane helix that anchors the domain in the membrane. In M160T9, nine C-terminal amino acids are missing, including one histidine,[13] and M160QT0 is the mutant where the methionine axial ligand has been replaced with glutamine.[44,45] Details of the protein preparation and purification are given in refs 13, 44, and 45. The concentrations of the M160T9 and M160QT0 samples were 1.5−3.0 mM Cu_A in 50% glycerol and 50% 100 mM phosphate/200 mM NaCl, pH 7. Two N_2-OR samples, both from *Pseudomonas stutzeri*, were studied. The first, labeled with ^{34}S, was isolated from the wild-type strain (ATCC 14405) grown with 0.25 mM $Na_2^{34}SO_4$ at a final concentration of 90 mg/mL in a solution of 50 mM Tris-HCl, pH 7.5. The second was from MK (His-auxotrophic strain) cells grown in L-histidine (40 μL) with a final concentration of 105 mg/mL in 50 mM Tris-HCl, pH 7.5.[46] Both yielded proteins with the same properties as confirmed by the experimental results. The enzyme was studied in its resting state where the Cu_A is

(24) Randall, D. W.; Gamelin, D. R.; LaCroix, L. B.; Solomon, E. I. *J. Biol. Inorg. Chem.* **2000**, *5*, 16−29.
(25) DeBeer-George, S.; Metz, M.; Szilagyi, R. K.; Wang, H.; Cramer, S. P.; Lu, Y.; Tolman, W. B.; Hedman, B.; Hodgson, K. O.; Solomon, E. I. *J. Am. Chem. Soc.* **2001**, *123*, 5757−5767.
(26) Olsson, M. H. M.; Ryde, U. *J. Am. Chem. Soc*. **2001**, *123*, 7866−7876.
(27) Malkin, R.; Malmström, B. G. *Adv. Enzymol*. **1970**, *33*, 177−244.
(28) Gewirth, A. A.; Cohen, S. L.; Schugar, H. J.; Solomon, E. I. *Inorg. Chem.* **1987**, *26*, 1133−1146.
(29) Lowery, M. D.; Guckert, J. A.; Gebhard, M. S.; Solomon, E. I. *J. Am. Chem. Soc.* **1993**, *115*, 3012−3013.
(30) Thomann, H.; Bernardo, M. *Methods Enzymol.* **1993**, *227*, 118−189.
(31) Neese, F.; Kappl, R.; Hütterman, J.; Zumft, W. G.; Kroneck, P. M. H. *J. Bioinorg. Chem.* **1998**, *3*, 53−67.
(32) Coremans, J. W. A.; Poluektov, O. G.; Groenen, E. J. J.; Warmerdam, G. C. M.; Canters, G. W.; Nar, H.; Messerschmidt, A. *J. Phys. Chem*. **1996**, *100*, 19706−19713.
(33) Coremans, J. W. A.; Poluektov, O. G.; Groenen, E. J. J.; Canters, G. W.; Nar, H.; Messerschmidt, A. *J. Am. Chem. Soc*. **1996**, *118*, 12141−12153.
(34) Gurbiel, R. J.; Fann, Y. C.; Surerus, K. K.; Werst, M. M.; Musser, S. M.; Doan, P. E.; Chan, S. I.; Fee, J. A.; Hoffman, B. M. *J. Am. Chem. Soc.* **1993**, *115*, 10888−10894.
(35) Deligiannakis, Y.; Louloudi, M.; Hadjiliadis, N. *Coord. Chem. Rev*. **2000**, *204*, 1−112.
(36) Jin, H.; Thomann, H.; Coyle, C. L.; Zumft, W. G. *J. Chem. Soc.* **1989**, *111*, 4262−4269.
(37) Kofman, V.; Farver, O.; Pecht, I.; Goldfarb, D. *J. Am. Chem. Soc.* **1996**, *118*, 1201−1206.
(38) Avigliano, L.; Davis, J. L.; Graziani, M. T.; Marchesini, A.; Mims, W. B.; Mondovi, B.; Peisach, J. *FEBS Lett.* **1981**, *136*, 80−84.
(39) Goldfarb, D.; Fauth, J. M.; Farver, O.; Pecht, I. *Appl. Magn. Reson.* **1992**, *3*, 333−351.
(40) Coremans, J. W. A.; Poluektov, O. G.; Groenen, E. J. J.; Canters, G. W.; Nar, H.; Messerschmidt, A. *J. Am. Chem. Soc*. **1996**, *118*, 12141−12153.
(41) Werst, M. M.; Davoust, C. E.; Hoffman, B. M. *J. Am. Chem. Soc*. **1991**, *113*, 1533−1538.
(42) Salgado, J.; Warmerdam, G.; Bubacco, L.; Canters, G. W. *Biochemistry* **1998**, *37*, 7378−7389.
(43) Jaszewski, A. R.; Jezierska, J. *Chem. Phys. Lett.* **2001**, *343*, 571−580.
(44) Slutter, C. E.; Gromov, I.; Epel, B.; Richards, J. H.; Pecht, I.; Goldfarb, D. *J. Am. Chem. Soc.* **2001**, *123*, 5325−5336.
(45) Slutter, C. E.; Gromov, I.; Richards, J. H.; Pecht, I.; Goldfarb, D. *J. Am. Chem. Soc.* **1999**, *121*, 5077−5078.
(46) Alvarez, M. L.; Ai, J.; Zumft, W.; Sanders-Loehr, J.; Dooley, D. M. *J. Am. Chem. Soc*. **2001**, *123*, 576−587.

oxidized, and the catalytic Cu_Z is EPR silent. The purpAz sample was obtained as reported,[10,11] and the protein concentration was 0.35 mM in 50 mM ammonium acetate, pH 5.1. The complexes of Cu(II) tetraimidazole (Cu−Imid) and Cu(II) bis-histidine (Cu−His) were prepared as described earlier,[47] and the Cu(II) concentration was 2 mM in 50:50 water:glycerol. Samples of all proteins and model compounds (total volume of 1−2 μL) were placed in EPR quartz tubes (0.8 OD) for all measurements.

Spectroscopic Measurements. W-band pulsed EPR and ENDOR measurements were carried out at 94.9 GHz and 4.5 K using a home-built spectrometer described elsewhere.[48] Field-sweep (FS) echo-detected (ED) EPR spectra were recorded using the two-pulse echo sequence ($\pi/2 - \tau - \pi - \tau -$ echo), where the echo intensity was registered as a function of the magnetic field. Typically, microwave (MW) pulse lengths (t_{MW}) of 0.09 and 0.18 μs were used with $\tau = 0.3$ μs. The magnetic field values were calibrated using the Larmor frequency of the protons, ν_H, as determined by the ENDOR measurements. The ^{1}H ENDOR spectra were measured using the Davies ENDOR pulse sequence ($\pi - T - \pi/2 - \tau - \pi - \tau -$ echo, with an RF pulse applied during the time interval T).[49] The experimental conditions for the Davies ENDOR spectra were $t_{MW} = 0.2$, 0.1, 0.2 μs, $\tau = 0.35-0.5$ μs, $t_{RF} = 25-40$ μs. In variable mixing time ENDOR experiments, an additional delay, t_{mix}, is inserted between the RF pulse and the echo detection sequence. The frequency scale in the ^{1}H ENDOR spectra is given with respect to the ^{1}H Larmor frequency. The repetition rate in these experiments, except for those stated otherwise, was 150 Hz.

Simulations. EPR simulations were carried out using a program developed by Neese.[50] ^{1}H ENDOR spectra were simulated using a program developed in our laboratory according to Erickson et al.[51] In this program, the hyperfine coupling tensor **A** is not limited to axial symmetry. The anisotropic part, given by **D**, was calculated for the Cu_A centers from the atomic coordinates using the point-dipole approximation as described by Neese.[50] For each proton denoted by i, $\mathbf{D}_i$ is obtained from contributions of six $\mathbf{D}^p_{i,j}$ ($j = 1, 6$) matrices, corresponding to the individual H_i-X_j interactions where $X_j = Cu_1$, Cu_2, S_1, S_2, N_1, N_2. The principal values of each $\mathbf{D}^p_{i,j}$ are ($-a_{\perp ij}$, $-a_{\perp ij}$, $2a_{\perp ij}$), where $a_{\perp ij} = (\mu_0/4\pi)\rho_j g_n \beta_n g\beta/(hr^3_{H_i-X_j})$, and ρ_j is the spin density on the X_j nucleus. The individual $\mathbf{D}_i$'s, expressed in the principal axis system of **g**, are then obtained by summing over all six dipolar interactions according to

$$\mathbf{D}_i = \sum_{j=1}^{6} \mathbf{D}_{ij} = \sum_{j=1}^{6} R(\theta_{ij}, \phi_{ij}) \mathbf{D}^p_{ij} R^{-1}(\theta_{ij}, \phi_{ij}) \qquad (1)$$

where θ_{ij} and ϕ_{ij} are the polar and azimuthal angles representing the orientation of the X_j-H_i vector with respect to the **g** principal axis system, and $R(\theta_{ij}, \phi_{ij})$ is the corresponding rotation matrix. Finally, the $\mathbf{D}_i$ were diagonalized to give the principal components of each coupled proton and the Euler angles, α, β, γ, relating it to the **g** frame. θ_0 and ϕ_0 describe the orientation of the external magnetic field, $\vec{B}$, with respect to the **g** principal axes system.

The orientation of g_{zz} was taken along the bisector of the two vectors normal to the $S-Cu_1-S$ and $S-Cu_2-S$ planes and that of g_{yy} parallel with the S−S direction.[50,52] The various θ_{ij}, ϕ_{ij}, and $r_{H_j-X_i}$ were calculated from the atomic coordinates of the 3-D structures, and the protons were placed using InsightII by MSI.

In the simulations, the selected orientations were determined as follows: the EPR spectrum was simulated, and using the **g** and ^{63,65}Cu hyperfine coupling constants, a plot of the resonant magnetic fields as a function of the angles θ_0 and $\phi_0 = 90°$, 0° was generated. Selected orientations were then determined graphically[53] assuming a line width of 100 G.

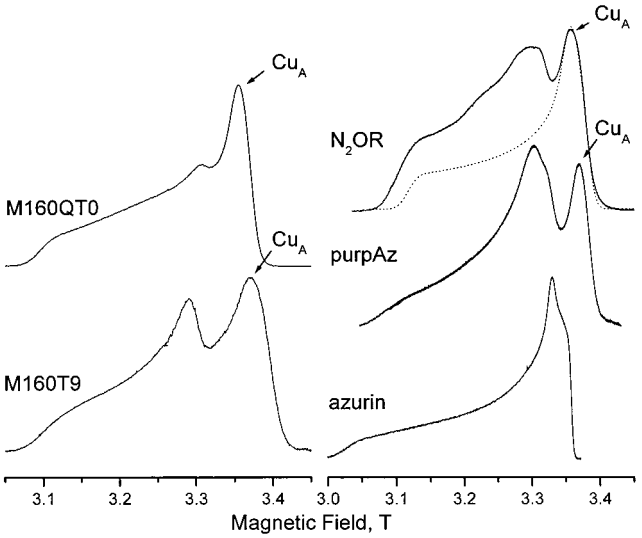

Figure 2. W-band FS-ED EPR spectra (4−5 K) of frozen solutions of N_2OR, purpAz, M160T9, M160QT0, and azurin. The dotted trace represents simulations obtained with the g-values listed in Table 1.

Table 1. g and $A_{\|}$(Cu) Values of the Different Cu_A and T1 Centers Investigated

	g_{xx}	g_{yy}	g_{zz}	$A_{\|}$, mT
N_2OR	2.005	2.02	2.175	4.28[a] [52]
M160T9[45]	2.0	2.02	2.189	3.1
M160QT0[45]	2.02	2.02	2.176	4.2
purple Az[11]	2.01	2.04	2.17	5.5
Azurin[61]	2.039	2.057	2.273	5.4[62]

[a] The average value of the two coppers (117 and 124 MHz) was taken.

Results

The W-band FS-ED EPR spectra of N_2OR, M160T9, M160QT0, purpAz, and azurin are presented in Figure 2, and the g-values determined from these spectra are summarized in Table 1. All spectra, except that of azurin, show, in addition to the $g_\perp$ feature of Cu_A (marked on the figure), a peak at ∼3.3 T which is assigned to the $g_\perp$ feature of a mononuclear Cu(II) center. Unlike X-band, at W-band the two centers are easily distinguished even at the $g_\perp$ region. In the case of M160T9, this feature was unambiguously assigned to a type II (T2) Cu(II) ion on the basis of X-band spectra measured at 160 K, where only the T2 spectrum is detected, and by simulations of the W-band spectrum using the Cu_A and T2 g-values.[44] On the basis of the similar position of the above extra feature, its different relative intensity and relaxation characteristics, we assign it also in purpAz, M160QT0, and N_2OR to a mononuclear Cu(II) "impurity" center. The $g_{\|}$ singularity of the Cu_A center is clear in all spectra, whereas that of the T2 is outside the displayed magnetic field range. The dotted line shows the simulated spectrum of the Cu_A of N_2OR calculated with the parameters given in Table 1. The spin−lattice relaxation time, T_1, of the

(47) Manikandan, P.; Epel, B.; Goldfarb, D. *Inorg. Chem.* **2001**, *40*, 781−787.
(48) Gromov, I.; Krymov, V.; Manikandan, P.; Arieli, D.; Goldfarb, D. *J. Magn. Reson.* **1999**, *139*, 8−17.
(49) Davies, E. R. *Phys. Lett. A* **1974**, *47*, 1−2.
(50) Neese F. Electronic Structure and Spectroscopy of Novel Copper Chromophores in Biology. Ph.D. Thesis, University of Konztanz, 1997.
(51) Erickson, R. *Chem. Phys.* **1996**, *202*, 263−275.
(52) Neese, F.; Zumft, W. G.; Antholine, W. G.; Kroneck, P. M. H. *J. Am. Chem. Soc.* **1996**, *118*, 8692−8699.
(53) Goldfarb, D.; Fauth, J.-M.; Tor, Y.; Shanzer, A. *J. Am. Chem. Soc.* **1991**, *113*, 1941−1948.

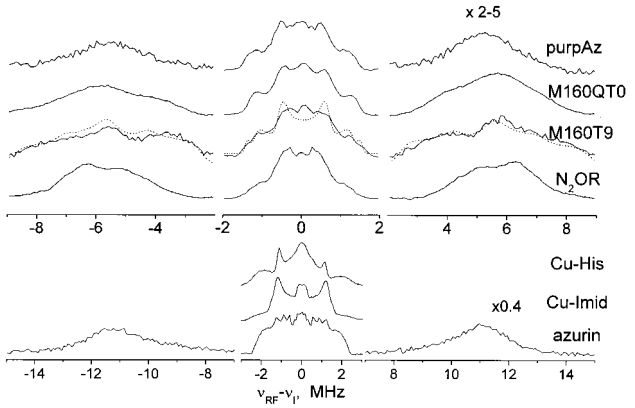

Figure 3. W-band ENDOR spectra, recorded at $g_\perp$ (4−5 K), of frozen solutions of N_2OR, purple azurin, M160T9, M160QT0, azurin, Cu−Imid, and Cu−His. The amplitude of the signals in the region of ±(3−14) MHz was scaled up for better visualization. The dotted lines are simulated spectra of M160T9 (fitting parameters are given in Table 2).

mononuclear Cu(II) is significantly longer than that of the Cu_A center, and, therefore, its relative contribution to the spectrum can be reduced by partial saturation, achieved by increasing the repetition rate from 150 Hz to 0.5−1 kHz. This has been used while recording the ENDOR spectra of N_2OR and purpAz. The only protein that contained a negligible amount of mononuclear Cu(II) is the M160QT0 mutant. This center may originate from the protein isolation process or from a time-dependent loss of copper from the Cu_A site to a nonspecific site where it is coordinated to a histidine residue (see below).[44] In the case of N_2OR, it may also originate from a partial reduction/decay of the EPR silent Cu_Z catalytic site which is a possibility supported by its different line shape. We rule out the possibility that the 3.3 T feature appears as a consequence of a line shape distortion because of echo detection because all spectra were recorded with the same MW power and pulse width, and yet this line is not observed in azurin and is very weak in M160QT0.

The ^{1}H ENDOR spectra of N_2OR, M160T9, M160QT0, and purpAz, recorded at the Cu_A $g_\perp$ position, where there are no interferences from the mononuclear Cu(II), are presented in Figure 3. Two types of protons are recognized. The first consists of protons with large, mostly isotropic hyperfine couplings in the range of 7−15 MHz attributed to the cysteine β-protons,[31,44] whereas the second comprises the weakly coupled protons with couplings smaller than 3 MHz. The resolution of the β-protons signals of N_2OR, M160T9, and M160QT0 allows the distinction of inequivalent protons (see next section). In contrast, the signals of the purpAz's β-protons are unresolved, exhibiting an average splitting of 10.8 MHz. For comparison, the spectrum of azurin recorded at g_{yy} is displayed as well. There, at $g_\perp$, the two cysteine β-protons are not resolved and have a coupling of 22.2 MHz, which is about twice the value observed for these protons in purpAz.

The ^{1}H ENDOR spectra of the weakly coupled protons of the Cu_A centers have, in general, similar line shapes. They differ mainly in the total width of the powder pattern, where the M160T9 spectrum exhibits the largest coupling. There, the outer edges exhibit two features with couplings of 2.8 and 2.3 MHz. In N_2OR and purpAz, these are reduced to 2.6 and 2.1−2.2 MHz, whereas in M160QT0 they almost merge into one feature with a splitting of 2.5 MHz. As expected, the width of the powder patterns of the weakly coupled protons of azurin is almost twice as large, 4.2 MHz.

The availability of the 3-D structures of three of the investigated proteins combined with well-resolved orientation selective sets of ENDOR spectra provide a unique opportunity to analyze the spectra on the basis of the 3-D structure. This leads to a more accurate determination of the spin density distribution and to the direct correlations between spectral features and structural parameters. Although the X-ray determined 3-D structure of these proteins does not provide proton coordinates, except for water molecules and OH groups, a good estimate of their positions can be obtained using well-known bond angles and lengths. Accordingly, we have employed InsightII (by MSI) to place the protons of the ligands of Cu_A center in their 3-D structures. Some of these protons are shown in the structures depicted in Figure 1. The coordinates of these protons were then used to estimate the various $\mathbf{D}_i$'s according to the procedure outlined in the Experimental Section. For example, Table 2 lists the D_{kk} ($k = x, y, z$) values of the β-protons of N_2OR and the Euler angles relating them with the **g**-frame.

In the case of N_2OR, the available 3-D structure has been determined on a crystal where the Cu_A is in the reduced state,[20] while the EPR measurements were all carried out on the resting, that is, mixed-valence state. The use of the coordinates of the reduced state is justified by the subtle structural changes the site probably undergoes upon reduction. This is based on studies of the structure of bovine heart COX, determined in both the reduced and the oxidized states.[19] The differences observed were rather limited, manifested mainly in a slight expansion of the reduced state with Cu−X bond length differences on the order of 0.05 Å and practically no change in the orientation of the ligand residues. Similarly, EXAFS measurements of reduced and mixed-valent states of the soluble Cu_A fragment of *Thermus thermophilus* and *Bacillus subtilis* resolved only minor changes in the core geometry.[54] These changes are insignificat with respect the structural differences among the different proteins. In the next two sections, the analysis of the ENDOR spectra of the β-protons and the weakly coupled protons is presented.

Cysteine β-Protons. Orientation selective ^{1}H ENDOR spectra of N_2OR are shown in Figure 4. The spectral region of the β-protons is free from mononuclear Cu(II) interferences because their large couplings are unique to the cysteine ligands in T1[41] and Cu_A centers.[31] We first attempted to reproduce the orientation dependence of the β-proton signals using the isotropic hyperfine values determined from earlier X-band ENDOR measurements[31] (13.3, 11.7, 10.4, 8.6 MHz for C561_1HB, C565_1HB, C561_2HB, C565_2HB, respectively) and the D_{kk} components listed in Table 2, calculated with ρ_S, ρ_{Cu}, and ρ_N values of 22, 25, and 3% on each Cu, S, and directly coordinated N, respectively. The latter are within the range found experimentally and predicted theoretically.[25,31,50] Earlier X-band EPR and ^{14}N ENDOR results showed that the spin densities on both coppers and two bound ^{14}N nuclei are close,[44,52] and we have, therefore, assumed the same ρ_S for both sulfurs. Changing the spin densities to 20, 27, and 3%, respectively, led to relatively insignificant variations in the range of ±0.05 MHz in the D_{kk} and ±0.5° in the angles. The simulated traces are displayed as dashed lines in the low-frequency part of Figure 4. The

(54) Blackburn, N. J.; de Vries, S.; Barr, M. E.; Houser, R. P.; Tolman, W. B.; Sanders, D.; Fee, J. A. *J. Am. Chem. Soc.* **1997**, *119*, 6135−6133.

Table 2. Hyperfine Interaction Parameters of the Cysteine β-Protons of the Proteins Investigated As Determined from the Best-Fit Simulations of the Orientation Selective ENDOR Spectra, As Compared to Values Calculated from the 3-D Structures[20] and $\rho_S = 22\%$, $\rho_{Cu} = 25\%$, $\rho_N = 3\%$ (in Parentheses)[a]

protein	proton	A_{iso} MHz	D_{xx} MHz	D_{yy} MHz	D_{zz} MHz	α deg	β deg
N_2OR	C561_1HB	13.8	−1.84(−2.14)	−1.36(−1.55)	3.2(3.69)	131(37.1)	52(32.9)
	C561_2HB	11.0	−1.92(−2.01)	−1.46(−1.56)	3.38(3.66)	118(148.9)	55(47.5)
	C565_1HB	12.2	−1.58(−1.93)	−1.23(−1.49)	2.82(3.42)	25(49.6)	126(163.3)
	C565_2HB	9.1	−1.67(−1.84)	−1.44(−1.50)	3.11(3.34)	142(166.5)	49(50.9)
M160T9	C149_1HB	10.0	−1.92(−2.12)	−1.46(−1.60)	3.38(3.72)	139(131.3)	49(26.3)
	C149_2HB	15.4	−1.84(−2.17)	−1.36(−1.52)	3.20(3.68)	−32(21.4)	58(44.3)
	C153_1HB	6.8	−1.67(−2.18)	−1.44(−1.55)	3.11(3.72)	44(57.0)	131(169.0)
	C153_2HB	12.2	−1.58(−2.08)	−1.23(−1.46)	2.82(3.54)	13(162.0)	128(138.0)
M160QT0	1	10.3	−1.92	−1.46	3.38	41	124
	2	13.3	−1.84	−1.36	3.20	33	126
	3	11.6	−1.58	−1.23	2.82	−13	58
	4	8.1	−1.67	−1.44	3.11	39	126

[a] The angle γ was omitted as it does not affect the spectrum because of the axial symmetry of **g**.

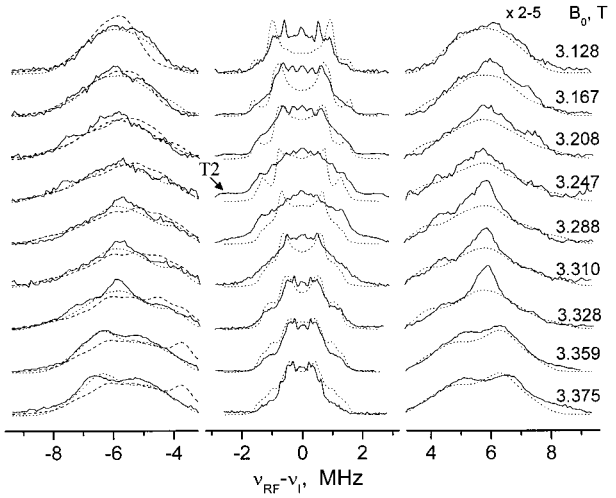

Figure 4. ^{1}H W-band ENDOR spectra of a frozen solution of N_2OR recorded at different fields along the EPR powder pattern (4.5 K). The amplitude of the signals in the region of ±(3−14) MHz was scaled up for better visualization. The dashed traces were calculated with the parameters listed in Table 2 and the A_{iso} values determined by Neese et al.[31] (see text). The dotted traces represent the best-fit simulated spectra calculated with the parameters listed in Table 2 for the cysteine β-protons, and in Table 6 for the weakly coupled protons. An individual line width of 0.9 MHz was used for the β-protons and 0.15 MHz for the others.

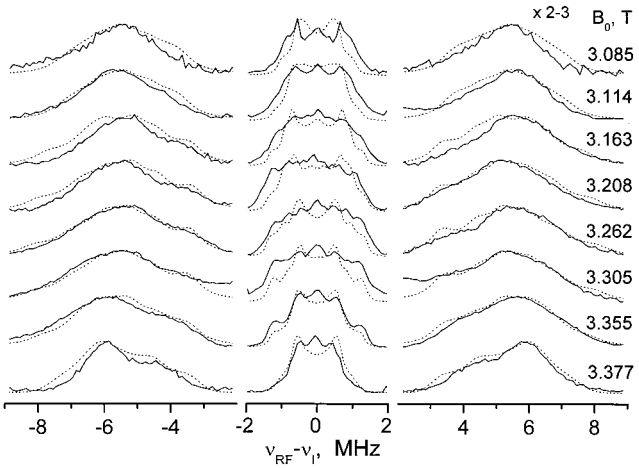

Figure 5. ^{1}H W-band ENDOR spectra of a frozen solution of M160QT0 recorded at different fields along the EPR powder pattern (4.5 K). The dotted traces represent the best-fit simulated spectra calculated with the parameters listed in Table 2 for the cysteine β-protons, and in Table 3 for the weakly coupled protons. An individual line width of 0.8 MHz was used for the β-protons and 0.15 MHz for the others.

agreement with the experimental total width of the high- and low-frequency components ($\Delta\nu_{\pm}(\beta)$) and the line shape is unsatisfactory. To improve the fit, both isotropic and anisotropic parts of the interaction had to be varied, and the best-fit simulated spectra are shown as dotted traces in Figure 4. The best-fit parameters, listed in Table 2, show that the A_{iso} values had to be adjusted and a reduction of 0.3−0.6 MHz in the D_{zz} value had to be introduced for some protons, as well as large changes in α and β. γ had no effect on the spectra because of the axial character of **g**.

A similar quality of fit could also be obtained with a set of negative A_{iso} values. The positive sign was determined from a series of variable mixing time ENDOR measurements reported elsewhere.[57] There, a long delay, t_{mix}, is introduced between the end of the RF pulse and the application of the echo-detection pulses.[55] At low temperatures, $t_{mix} \approx T_1$, and negligible cross or nuclear relaxation, the ENDOR signals corresponding to the $M_S = {}^1/_2$ manifold lose intensity and may even reach a negative amplitude.[55,56] This allows the identification of the ENDOR signals belonging to the different M_S manifolds and thereby the determination of the sign of the coupling. The ENDOR spectrum of N_2OR recorded at the Cu_A $g_{||}$ position as a function of t_{mix} exhibits a decrease in the relative intensity of the low-frequency components of the β-proton doublets and assigns them to the $M_S = {}^1/_2$ manifold, yielding $A_{iso} > 0$.[57] The positive shift of these protons in NMR spectra is consistent with this assignment.[42,58]

Orientation selective ENDOR spectra of M160QT0 are shown in Figure 5. The spectra are, in general, similar to those of N_2-OR; the resolution is lower, and $\Delta\nu_{\pm}(\beta)$ is slightly larger. Because there is no 3-D structure available for this mutant, we used the D_{kk} values obtained from the best-fit simulations of N_2OR and fitted A_{iso} and the angles. This was done under the assumption that the D_{kk} are primarily determined by the S−H distance, which does not vary from structure to structure, although ρ_S may vary and change somewhat the D_{kk} values. In addition, the relatively large individual line width which is on

(55) Bennebroek, M. T.; Schmidt, J. *J. Magn. Reson.* **1997**, *128*, 199−206.
(56) Epel, B.; Pöppl, A.; Manikandan, P.; Vega, S.; Goldfarb, D. *J. Magn. Reson.* **2001**, *148*, 388−397.
(57) Epel, B.; Manikandan, P.; Kroneck, P. M. H.; Goldfarb, D. *Appl. Magn. Reson.* **2001**, *21*, 287−297.
(58) Luchinat, C.; Soriano, A.; Djinovic-Carugo, K.; Saraste, M.; Malmström, B. G.; Bertini, I. *J. Am. Chem. Soc.* **1997**, *119*, 11023−11027.

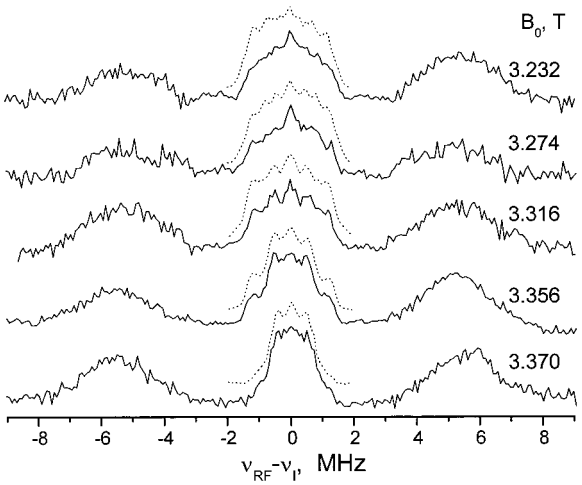

Figure 6. ^{1}H W-band ENDOR spectra of a frozen solution of purpAz recorded at different fields along the EPR powder pattern (4.5 K). The dotted traces show the spectra of the weakly coupled protons of M160QT0 recorded at similar fields.

the order of D_{yy} makes the simulations less sensitive to the D_{kk} values. The simulated spectra are presented as dotted traces in Figure 5, and the simulation parameters are listed in Table 2. A comparison with the values obtained for N_2OR shows a reduction in A_{iso} of some protons.

Unlike N_2OR, the orientation selective ENDOR spectra of the β-protons of purpAz did not show any features that could be used to distinguish the different protons (see Figure 6). Moreover, the splitting remained practically constant at 10.8 MHz throughout the field range of the EPR spectrum. From the line width and by comparison with the M160QT0 spectra, we estimated the maximum and minimum A_{iso} values as 12.5 and 9 MHz, respectively. Unfortunately, we were not able to obtain orientation selective spectra for M160T9 with a reasonable S/N, yet we have used the same strategy applied for M160QT0 to simulate the spectrum recorded at $g_\perp$, and we obtained the values of A_{iso}. The best-fit simulated trace is shown as a dotted trace in Figure 3, and the parameters used are listed in Table 2. This spectrum was simulated previously with similar negative A_{iso} values,[44] but on the basis of the N_2OR results described above, we concluded that the couplings are positive in all Cu_A centers.

Weakly Coupled Protons. The strategy we adopted in the analysis of the weakly coupled protons differed from the case of the β-protons, where best-fit simulations were carried out, for the following reasons: (i) in a significant number of spectra there are interferences from a mononuclear Cu(II) ion center, (ii) the number of protons contributing to this spectral region is relatively high, (iii) the relative intensities of peaks very close to the Larmor frequency are underestimated because of the limited selectivity of the MW pulses. We have, therefore, concentrated on reproducing the total width of the spectra with emphasis on the region of $\pm$0.5 MHz and up, where the contribution of more distant protons and the effect of the MW pulse nonselectivity become negligible. In all cases, except M160QT0, we started with the dipolar interactions calculated from the 3-D structures, and, whenever required, the agreement with the experimental results was improved by changing the spin densities, adding isotropic coupling constants. If this did not yield satisfactory results, mild changes in the angles were introduced.

Table 3. Anisotropic Hyperfine Tensors of Weakly Coupled Ligand Protons in the Cu_A Site of the Proteins Studied with D_{zz} Values Higher than 2 MHz As Calculated from the 3-D Structures for $\rho_S = 22\%$, $\rho_{Cu} = 25\%$, $\rho_N = 3\%$[a]

protein	proton	A_{iso}[c] MHz	D_{xx} MHz	D_{yy} MHz	D_{zz} MHz	α deg	β deg
PurpAz[b]	H120_HE1		−1.69	−0.85	2.54	−11.9	92.0
	H120_2HB		−1.52	−0.80	2.33	6.6	102.6
	H120_HA		−1.50	−1.01	2.50	−168.2	145.3
	C116_H		−1.44	−0.91	2.35	−3.5	113.5
	H46_HE1		−1.64	−0.73	2.37	−5.5	80.3
	H46_HA		−1.84	−0.96	2.80	4.9	131.8
N_2OR	H526_HA		−1.3	−0.91	2.21	173.6	27.4
	H526_HE1		−2.14	−0.94	3.08	3.6	86.4
	W563_H		−1.58	−1.26	2.83	−7.6	51.6
	H569_HE1		−1.93	−0.83	2.76	−15.2	100.3
	M572_1HE		−1.17	−1.08	2.25	42.4	116.5
	C565_H	−0.9	−2.44	−1.16	3.6	−9.5	66.2(60)
M160T0	H114_HE1		−1.72	−0.77	2.49	−12.2	80.1
	H157_HA		−1.77	−1.12	2.88	−169.0	32.1
	H157_HE1	0.2	−1.91	−0.87	2.78	−11.4	91.1
	G151_H	−0.3	−1.53	−1.18	2.71	6.9	120.6
	C153_H	−1.3	−1.79	−1.02	2.82	3.5	114.9
M160QT0	1	−0.1	−1.9	−1.1	3.0	20	60
	2	−0.6	−2.3	−0.4	2.7	0	45
	3	0	−1.4	−0.9	2.7	70	30
	4	−0.7	−2.0	−0.5	2.5	20	30
	5	0.0	−1.5	−1.1	2.6	0	70

[a] The values in parentheses indicate the values used in the simulations, if different than the calculated ones. [b] The coordinates of molecule A were used. [c] Determined from simulations of the spectra.

We begin the analysis of the weakly coupled protons with the ENDOR spectra of M160QT0 because it is the only protein in the series investigated where the spectra are practically free from "impurity" signals throughout the full EPR spectral range. In this case, the 3-D structure is not available, and we attempted to fit the spectral features with couplings larger than 1 MHz. Table 3 shows that in all proteins a relatively large number of protons are expected to contribute to this spectral region. In all cases, $D_{zz} < 3.6$ MHz, which can be used as an upper limit. In addition, we took into consideration that in all structures the histidine $H_{\epsilon 1}$ protons are expected to have relatively large couplings (D_{zz} is in the range of 2.4−3.0 MHz and $\beta = 90 \pm 10°$) and that they should have major contributions to the outer wings ($A_{max} = 2.6$ MHz) in spectra recorded close to $g_\perp$. Other protons that are close to the Cu_2S_2 core in all structures are the amide proton of one of the cysteines and the α-proton of one of the histidines. These protons are characterized by $\beta < 70°$, and, therefore, their maximum hyperfine coupling should be observed at $\theta_0 < 90°$.

We first fitted the A_{max} features of the 3.377 and 3.355 T with a proton having $H_{\epsilon 1}$ characteristics. The experimental spectra (Figure 5) shows that a second proton, with $A_{max} = 2.6$ MHz that is reached toward the center of the EPR powder pattern, is present as well. The relatively high intensity of this feature indicates that it corresponds to an A_{xx} or A_{yy} singularity, rather than to A_{zz}. Such features can be obtained from a proton with an $A_{iso} < 0$ and $\beta \approx 25-45°$. The fit was improved by adding three more protons. The final simulation with all five protons is compared with the experimental set in Figure 5, and the best-fit parameters are listed in Table 3. The total width of the spectra is reasonably reproduced, but the fit of the peaks' position and relative intensity varies. This is expected because not all protons have been taken into account, and the sensitivity of Davies ENDOR to larger couplings has been neglected. Protons 1 and 5 have the largest values of β and are, therefore,

assigned to the two histidines' $H_{\epsilon 1}$. The protons with the relatively large negative A_{iso} (no 2 and 4) can be assigned to (i) the amide proton C153_H because of the large spin density on S and the finite spin found on a backbone nitrogen[44] and (ii) to the α-proton of H157 because of its angle β and its close distance to the Cu_2S_2 in M160T0 (see Table 3). The possibility that it can also be one of the NH_2 protons of the replacing glutamine cannot be ruled out, however.

The spectra of purpAz and M160QT0 recorded within the range 3.37−3.31 T are almost identical. Attempts to simulate the M160QT0 spectra using the calculated **D** obtained from the 3-D structure of purpAz (see Table 3) while varying the A_{iso} values did not produce the overall width of the spectra. Comparison of calculated values for purpAz with those obtained by fitting the M160QT0 spectra shows that the dipolar couplings calculated for purpAz are too small to fit the experimental results. It was possible to obtain D_{kk} values that agree better with the experimental results by changing ρ_S, ρ_{Cu}, and ρ_N to 15, 32, and 3%, respectively. This gave larger D_{zz} values for the histidine $H_{\epsilon 1}$ protons (increase to 2.90 and 2.38 MHz) without varying significantly those of the other protons.

The ENDOR spectra of the weakly coupled protons of N_2-OR, shown in Figure 4 and measured within the range B_0 = 3.129−3.248 T, contain contributions from both Cu_A and the mononuclear Cu(II) impurity. The most apparent contributions of the latter are the clear singularities at ±2.5 MHz in the spectra recorded at B_0 = 3.167−3.248 T (see arrow in Figure 4). This assignment was substantiated by recording the spectra with a faster repetition rate, which leads to a partial saturation of the mononuclear Cu(II) EPR signal, while that of the Cu_A is less affected because of the difference in spin−lattice relaxation times. Under these conditions, the intensities of the ENDOR peaks at ±2.5 MHz were reduced significantly. These signals correspond to an A_{zz} value of ∼5 MHz which suggests that they arise from the imidazole protons of a remote Cu(II) binding histidine residue. This assignment is supported by comparison with the ENDOR spectra of azurin and of the Cu−Imid and Cu−His complexes, that can serve as models for the coupling of the imidazole protons (see Figure 3). The A_{zz} values of these models[47,56] are about twice those observed for the Cu_A centers, as expected considering the spin distribution over two coppers in Cu_A. These signals are also clear in purpAz (see Figure 6). They were also observed in earlier X-band ENDOR spectra of N_2OR where they have been assigned to unknown protons in the Cu_A center.[31]

The weak coupling regions of the ENDOR spectra of N_2OR were simulated using the calculated **D** parameters of the protons in the vicinity of the Cu_2S_2 core listed in Table 3 (except for H526_HA which has the smallest predicted D_{zz} value). The major discrepancy between the calculated and experimental spectra was the absence of an intensity at ±1.4 MHz in spectra recorded with field settings in the center of the EPR powder pattern. Comparison with the spectra of M160QT0 (see above) strongly suggests that these features arise from a Cu_A proton with a substantial negative A_{iso} and value of $\beta \approx 45°$. Consequently, finite A_{iso} values were tried for the amide protons C565_H and W563_H. Setting $A_{iso} = -0.9$ MHz for C565_H and changing β from 66° to 60° improved the fit significantly, whereas the introduction of A_{iso} for W563_H led to large deviations at 3.359 T, where mononuclear Cu(II) does not interfere. The simulated spectra are shown in Figure 4.

The simulations of the weakly coupled protons along with the dipolar couplings calculated from the 3-D structures show that the splitting of the outer wings in spectra recorded around $g_\perp$ is determined primarily by the two $H_{\epsilon 1}$ protons, although some contributions from a proton with $A_{iso} \approx (-0.5) - (-0.7)$ MHz with a small β (like proton 4 in M160QT0) may also be significant. The outer wings in the $g_\perp$ ENDOR spectrum of M160T9 appear at 2.8 and 2.3 MHz, which is slightly larger than that observed for N_2OR and M160QT0. Simulations were carried out using the calculated D_{kk} values and orientations determined from the structure of M160T0, listed in Table 3, and splitting of the outer edges in the simulated spectrum was too small. Although the 3-D structure was determined for M160T0, the similar spectroscopic properties of M160T0 and M160T9[44] justify the assumption that the structure of the Cu_A center has not changed by the removal of the nine terminal amino acids. A better fit could be obtained by introducing A_{iso} = 0.2 MHz to H157_HE1. A similar quality fit could be obtained by setting $A_{iso} = 0$ and ρ_S, ρ_{Cu}, and ρ_N to 18, 30, and 2%, respectively, but the higher $A_{||}$(Cu) values of N_2OR make the first option more attractive. In addition, in light of the spectral analysis of M160QT0 and N_2OR, we introduced A_{iso} = −1.3 MHz for the amide proton C153_H. This did not increase the maximum splitting but improved the fit of the relative intensity of the feature at ±1.15 MHz. An $A_{iso} = -0.3$ MHz was also taken for G151_H. A comparison between the simulated and experimental spectra is presented in Figure 3.

Discussion

Generally, the ENDOR spectrum reflects the spin density distribution in the paramagnetic center. An unambiguous determination of these densities does, however, require the knowledge of the 3-D structure. The simulations of the orientation selective ENDOR spectra of the cysteine β-protons of N_2OR showed that the calculated D_{zz} values based on the 3-D structures and using ρ_S = 22%, ρ_{Cu} = 25%, and ρ_N = 3% are overestimated by 10−20% relative to the D_{zz} value obtained from best-fit simulations of the orientation selective ENDOR spectra (see Table 2). Moreover, the same smaller D_{zz} values reproduced the spectra of the β-protons of M160QT0 and M160T9. Because the major contribution to the anisotropic hyperfine interaction of these protons arises from the S^γ−H distance, this discrepancy can be ascribed to an overestimation of ρ_S. However, reducing ρ_S means increasing ρ_{Cu} or ρ_N, which would in turn lead to an increase of the hyperfine coupling of the $H_{\epsilon 1}$ protons (see below) and to a disagreement with the experimental results. Consequently, we attribute the overestimate in the calculated D_{zz} values to the use of the point-dipole approximation which may not be fully appropriate for an S−H distance of 2.3 Å. Another possibility is an error in the proton coordinates because of the limited resolution of the X-ray diffraction data used to determine the structure (2.4 Å in the case of N_2OR). In the case of the β-protons, the deviation in D_{zz} means an error of about +0.1 Å in the S^γ−H distance.

The simulation of the orientation selective spectra gave the A_{iso} values of the β-protons, which are related to the H−C−S−S dihedral angle, ϕ, according to[31]

$$A_{iso} = \rho_S(B \sin^2 \phi + C) \qquad (2)$$

where B represents the part of A_{iso} that results from hyperconjugation and is orientation dependent, whereas C is a measure

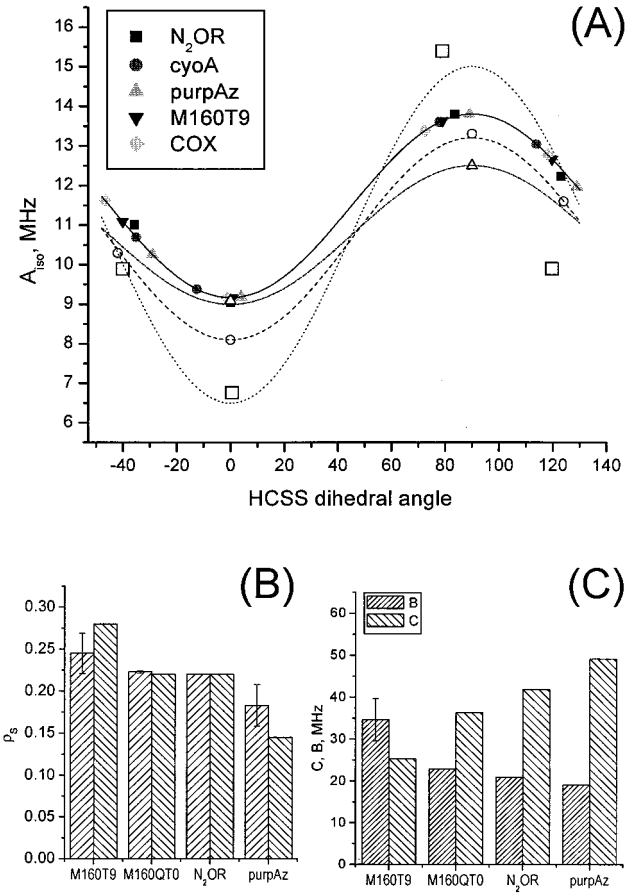

Figure 7. (A) Plot of A_{iso} of the cysteine β-protons as a function of the H−C−S−S dihedral angle. The solid line was obtained by fitting the experimental A_{iso} values of N_2OR, denoted by ■, to eq 2. All of the rest of the solid symbols are calculated A_{iso} obtained using the $\rho_S B$ and $\rho_S C$ values of N_2OR and the dihedral angles obtained from the 3-D structures of COX,[18] CyoA,[9] M160T0,[21] purpAz.[20] The dotted line and the □ represent the fit of M160T9, and the dashed line and the △ correspond to purpAz. The dashed−dotted line represents the fit to M160QT0 (○), where the values of $\rho_S B$ and $\rho_S C$ were determined using the minimum and maximum experimental values of A_{iso} assuming angles of 0 and 90°, whereas the other two angles where determined from the fit. (B) ρ_S values of the proteins investigated calculated using the two approaches described in the text. (The error bars were estimated by taking $A_\perp(Cu) = 1$ mT rather than 2 mT.) (C) The values of B and C of the various proteins.

of the contribution of other mechanisms such as spin polarization. Figure 7A shows the dependence of the A_{iso} values of N_2-OR on the ϕ angles that were obtained from the 3-D structure,[20] and fitting of the data to eq 2 yields $\rho_s B = 5.2$ MHz and $\rho_s C = 9.0$ MHz. We then calculated the predicted A_{iso} values of the β-protons of four other Cu_A centers from their dihedral angles[9,12,18,21] and using the same $\rho_S B$ and $\rho_S C$ values as in N_2-OR, and added them to the plot in Figure 7A. It shows that the dihedral angles are rather well conserved, exhibiting a variation of only ±7°. For two of the protons, ϕ is around 0° and 90°, and, therefore, they exhibit the maximum and minimum values of A_{iso} ($(A_{iso})_{max}$, $(A_{iso})_{min}$). In these orientations, slight changes in ϕ do not have a significant effect on A_{iso} because of the behavior of the $\sin^2\phi$ function. Consequently, the small errors in ϕ caused by the limited resolution of the X-ray data are not expected to significantly affect the extracted $\rho_s B$ and $\rho_s C$ values. Furthermore, the total width of the ENDOR signals of the four β-protons, $\Delta\nu_\pm(\beta)$, which is determined primarily by the spread in A_{iso} values rather than by the hyperfine anisotropy, can be

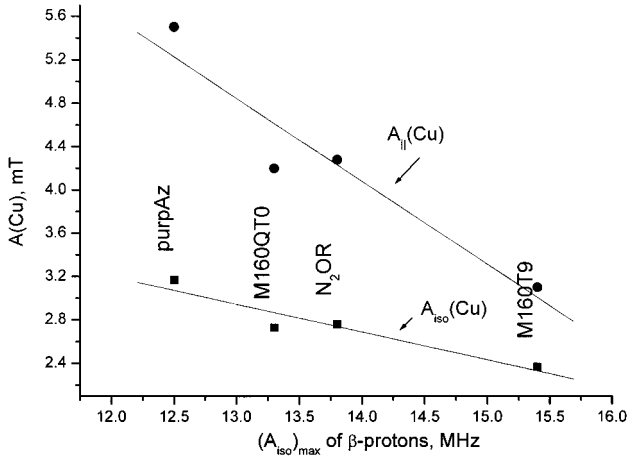

Figure 8. The correlation between the maximum A_{iso} value of the β-cysteine protons, $(A_{iso})_{max}$ and $A_{iso}(Cu)$, and $A_{||}(Cu)$ for the various Cu_A centers investigated.

used to estimate $\rho_S B$ and $\rho_S C$. Accordingly, the unresolved signals of purpAz only for the estimation of the extreme A_{iso} values, yielding $\rho_S B \approx 3.5$ MHz and $\rho_S C \approx 9$ MHz.

The extreme A_{iso} values of M160QT0, 13.3 and 8.1 MHz, yield $\rho_S B = 5.1$ MHz and $\rho_s C = 8.1$ MHz. Using these values, we present the dependence of A_{iso} on ϕ in Figure 7A by the dashed line, and the experimental A_{iso} values of the other two protons yield $\phi = -42°$ and 124° which are very close to those of the native protein, M160T9 (−40.1°, 119.7°). Fitting the A_{iso} values of M160T9 to eq 2 gave $\rho_S B = 8.5$ MHz and $\rho_S C = 6.5$ MHz (see dotted trace in Figure 7A). The fit is not as good as in N_2OR because only one ENDOR spectrum was used in the simulations, and, therefore, the experimental values are less accurate.

The simulations of the ENDOR spectra, through the anisotropic part of the hyperfine interaction and 3-D structure, provided a good estimate of the spin densities. However, because the resolution, purity, and availability of the orientation selective ENDOR spectra varied among the proteins examined, we have used the copper hyperfine interaction to refine their relative spin densities. A plot of the $(A_{iso})_{max}$ value of β-protons versus the observed $A_{iso}(Cu)$ or $A_{||}(Cu)$ of the investigated proteins shows a linear dependence with a negative slope (see Figure 8). This correlation is consistent with $(A_{iso})_{max}$ being proportional to ρ_S, and $A_{iso}(Cu)$ and $A_{||}(Cu)$ to ρ_{Cu}, where $\rho_S + \rho_{Cu} \simeq$ constant. This is also in agreement with recent density functional theory (DFT) calculations.[26] Furthermore, it indicates that the $(B + C)$ values of all proteins are rather close. The ENDOR data of N_2OR were the best in terms of resolution and completeness, and, therefore, spin densities of all other proteins were scaled relative to $\rho_{Cu}(N_2OR) = 25\%$, as determined from the ENDOR simulations. Next, we calculated the relative ρ_{Cu} of all proteins from the copper hyperfine interaction, where $A_{iso}(Cu)$ values were calculated from the $A_{||}(Cu)$ values listed in Table 1, and taking $A_\perp(Cu) = 2.0$ mT for all proteins.[59] Two approaches were employed to calculate the relative ρ_{Cu} values. In the first, we simply scaled ρ_{Cu} according to the $A_{iso}(Cu)$ values: $\rho_{Cu}(x) = A_{iso}(Cu)(x)\rho_{Cu}(N_2OR)/A_{iso}(Cu)(N_2OR)$. In the second approach,

(59) The $A_\perp(Cu)$ splittings are usually not resolved in the EPR spectra of the Cu_A centers, and the line width in this region looks similar in all proteins. Therefore, we have used the average value of the two copper ions, determined from simulations of the multifrequency EPR spectra of N_2-OR,[52] for all proteins.

the relative spin density was scaled using the expressions given for α^2, the spin density in the Cu $-|A_1; x^2 - y^2 > -|A_2; x^2 - y^2 >$ molecular orbital, as outlined by Neese,[50] that takes into account ($A_{||}$(Cu) $- A_{\perp}$(Cu)) and the *g*-values. In this case, we set $2\rho_{Cu}(N_2OR) = \alpha^2(N_2OR) = 2*0.25$. The ρ_S values of each protein, obtained using the two approaches and $\rho_S = [0.50 - (\rho_{Cu} + \rho_N)]$ with $\rho_N = 3\%$, are presented in Figure 7B. The difference between the two sets is small, both showing the same trend. This is consistent with the trend observed in simulations of the weakly coupled protons, although the actual numbers may vary. Finally, the values of the *B* and *C* parameters were calculated using the average ρ_S value for each protein, and they are displayed Figure 7C. The observed trend indicates an inverse relation between *B* and *C*. When the former increases, the latter decreases.

The ρ_S value obtained for purpAz, 14.5−18.3%, is smaller than that reported recently for the same protein (23%) using S-, K-edge XAS.[25] Recent DFT calculations on an optimized cluster with a structure similar to that of Cu_A in bovine COX gave $\rho_{S_{1,2}} = 21, 27\%$ and $\rho_{Cu_{1,2}} = 18, 27\%$.[26] Other DFT calculations, based on the structure of purpAz, report for $\rho_{Cu_{1,2}} = 23, 25\%, 20, 22\%$, and 21, 23% and for $\rho_{S_{1,2}} = 18, 26\%$, 22, 30%, and 20, 30%, depending on the calculation method.[25] The large difference in the ρ_{Cu} values of the two copper ions is also in disagreement with the EPR spectra of the presently investigated proteins where ^{63,65}Cu hyperfine couplings of two coppers ions are practically equivalent (see Table 1).

Unlike the cysteine β-protons, analysis of the weakly coupled protons has been limited by the overlap of a relatively large number of protons with similar hyperfine coupling characteristics. In addition, interferences from mononuclear Cu(II) overlapping signals present in three out of the four proteins investigated added difficulties. Nonetheless, the splittings of the outer wings of the spectra recorded at $g_{\perp}$ provide an estimate of the A_{zz} values of the histidine $H_{\epsilon 1}$ protons, which are sensitive to the geometry and to ρ_{Cu} more than to ρ_S and ρ_N. Because the EPR spectra[11,44,52] show that ρ_{Cu} is practically similar for the two copper ions, differences in the two $H_{\epsilon 1}$ protons are attributed primarily to geometrical variations between the two histidines. Consequently, any splitting in the outer wings of the spectra indicates different orientations/distances of the imidazole ligands with respect to the Cu_2S_2 core. While comparison of the difference between the calculated D_{zz} values of the two histidines $H_{\epsilon 1}$ is 0.32 MHz (N_2OR) > 0.29 MHz (M160T0) > 0.17 MHz (purpAz), the experimental trend shows M160T9 (0.35 MHz) > N_2OR (0.25 MHz) > purpAz (0.1−0.15 MHz) > M160QT0 (∼0.05 MHz). The larger, unexpected difference in M160T9 is attributed to the small finite and positive A_{iso} for one $H_{\epsilon 1}$, as was found by the simulations. Although the model we used to calculate the anisotropic hyperfine tensor is rather simplistic, because it considers the spin densities at six localized point centers rather than an integration over the whole wave function, it does provide guidelines on how the anisotropic hyperfine interaction will change with the geometry and spin-density distribution. Unlike other protons, the calculated D_{zz} values of the $H_{\epsilon 1}$ clearly increase with ρ_{Cu}. The effects of the geometrical changes are, however, difficult to isolate because a rotation of the imidazole about any axis leads to a significant variation of the Cu/S−H distance. This is well manifested in variations of up to 0.7 MHz (25%) in the calculated values of D_{zz} of the $H_{\epsilon 1}$ protons in M160T0(9), N_2OR, and purpAz (obtained for the same spin-density distribution).

The 3-D structures also predict the following trend for the $H_{\epsilon 1}$ with the maximum D_{zz}: N_2OR > M160T0(9) > purpAz (using the same ρ_{Cu} for all), whereas the experimental trend is M160T9 > N_2OR > purpAz ≈ M160QT0. The interchange of M160T0 and N_2OR is again attributed to the A_{iso} of one of the $H_{\epsilon 1}$ in M160T9. It is, however, unclear what the geometrical features are that lead to this small, but finite A_{iso} in this site and not in the others. The relatively low calculated D_{zz} value for $H_{\epsilon 1}$ of purpAz as compared to the experimental result is attributed primarily to the use of too small a value of ρ_{Cu} in the calculations and less to an experimental error in the proton coordinates. This is in agreement with a relatively large $A_{||}$(Cu) and the rather small coupling of the cysteine β-protons which indicates that ρ_{Cu} is higher in purpAz than in M160T9 and N_2-OR (see Figure 7B). The similarity between the M160QT0 and purpAz spectra in the region of the small coupling suggests that the M to Q mutation resulted in a more symmetric structure where the imidazoles have orientations similar to those in purpAz. We cannot resolve, however, if it involved H114 displacement into the core plane or an H151 movement out of it (see Figure 1). Still, the overall distances should be shorter than in purpAz because ρ_{Cu} is smaller as deduced from the lower $A_{||}$(Cu) value and the larger coupling of the β-protons.

Before discussing the implication of the trends in spin densities presented above, we summarize the approximations and assumptions made in the calculations. (i) The anisotropic hyperfine interaction was calculated by using a superposition of six point dipoles rather than averaging over the complete wave function. (ii) The small spin density on the directly bound nitrogens was assumed to be the same for both imidazoles and set to be 3% in all proteins. This was justified by calculations of **D** that showed that the effect of ρ_N on the proton couplings is insignificant. (iii) The same ρ_S values were taken for the two thiolates and justified by the good fit of the A_{iso} values of the β-protons to the relation given in eq 2. (iv) Similarly, the ρ_{Cu} on both copper ions was set to be the same on the basis of the EPR spectra. (v) The spin densities estimated from the ENDOR simulations were further scaled according to the copper hyperfine interaction, which was supported by the linear correlation of the β-protons $(A_{iso})_{max}$ and A_{iso}(Cu) (and $A_{||}$(Cu)). (vi) The 3-D structure used for N_2OR is that of the reduced Cu_A center, in which at least the Cu_A center of COX was found to be highly similar to that of the mixed-valence state.[19]

In the following, we attempt to correlate the observed trends in ρ_S with isolated structural features in the Cu_A sites such as Cu−Cu, Cu−S, and the Cu−weak ligand distances, the hinge angle of the Cu_2S_2 core, or the orientation of the imidazoles. DFT calculations gave a B_{3u} orbital ground state, which is σ^* with respect to the Cu−Cu axis, and ρ_S decreases with increasing Cu−Cu distance.[26] The difference in the Cu−Cu distance (2.51 Å (M160T0)[21] and 2.47 Å (N_2OR)[20]) is, however, too small to account for the ρ_S difference.[26] A close examination of the N_2-OR and M160T0 structures (see Figure 1) reveals that significant differences are the larger hinge angle in N_2OR and a significantly shorter Cu−N bond in M160T0. The shorter Cu−N distance should attract spin density from the S, rather than increase it. Consequently, the lower ρ_S in N_2OR could originate from the large hinge angle of the core. The purpAz structure exhibits more differences relative to the other two. The hinge

angle is the closest to 180° (similar to M160T0), but the orientation of one of the imidazoles is significantly different. Moreover, the distances between the copper ions and the weak ligands are significantly different. One of the copper ions has two weak ligands at a distance of 3−3.1 Å, and the other has one weak ligand at 2.2 Å. The distances in the case of M160T0 and N_2OR are 2.46,2.62 Å and 2.47,2.60 Å, respectively. According to Randall et al.,[24] an increase in the weak ligand interaction, caused by the reduced distance, should lead to an increase in the Cu−Cu distance and to a decrease in ρ_S. Hence, in purpAz there are two opposite trends, the shorter distance to E114 should decrease ρ_S and increase the Cu−Cu distance, whereas the increase in the distance to M123 should increase ρ_S. The lowest ρ_S in purpAz suggests that the effect of E114 dominates although the Cu−Cu distance in purpAz, 2.42 Å, is not significantly longer than in the others. The above discussion shows that there are actually many structural features in the Cu_A site that can be slightly modified and used to tune the ground state. These are complex, and understanding their explicit effect on the spin density distribution requires systematic quantum chemical calculations. The detailed information we obtained on the hyperfine couplings of the β-protons and on some of the weakly coupled protons for a series of Cu_A centers sets experimental constraints that can be used for further improvement of the DFT determined ground state.

We finally discuss the trends detected in the spin densities in terms of ET properties. DeBeer-George et al.[25] have calculated possible ET pathways in COX and noted the highly anisotropic redox active orbital with the sulfur bonds being the most covalent. This is highly relevant because the metal−ligand covalency is important, and the electron-transfer rate must be weighted by the appropriate ligand character in the redox active site. These authors calculated three possible pathways for the Cu_A to heme-a ET, and showed that when the covalency factor is taken into account, the path through one of the cysteines becomes competitive with the shorter path going through one of the imidazole ligands. Therefore, on the basis of our results, the higher covalency factor is expected for M160T9, and the lower is expected for purpAz. This, however, is only one out of several factors that determines the ET rate, and comparative experimental results which isolate the various contributions in the different studied proteins are not available. Consequently, at present this correlation cannot be checked experimentally.

The ENDOR spectra of all investigated Cu_A centers showed the presence of a proton with a negative A_{iso} interaction. There are two candidate sites for this proton. One is the amide of one of the cysteines, which is closer to the Cu_2S_2 core, and its orientation is conserved in all structures, as shown in Figure 1. The second is the α-proton of one of the histidines, which in all structures seems to be close to the Cu_2S_2 core. The first option is more likely because in all proteins a weakly coupled amide nitrogen with $A_{iso} \approx (1-1.3)$ MHz has been detected. In M160T9, M160QT0,[44] and purplAz,[60] it was clearly observed in HYSCORE spectra, whereas in N_2OR it was detected in the three-pulse ESEEM spectrum.[36] This nitrogen was assigned to the amide of the cysteine that is bent over the core as opposed to the second one that is oriented away from the core.[44] It is, therefore, expected that the amide proton will also exhibit some isotropic coupling. The cysteine residue that is bent over the core in COX is C200.[17,18] A recently proposed ET pathway calculated for bovine COX suggests that C200 takes part in the input path of the electron from cytochrome *c*.[25] Hence the A_{iso} values of the amide nitrogen and proton may be significant for the ET efficiency.

The finite isotropic hyperfine interaction observed for a number of rather remote protons and nitrogens shows that the spin distribution goes far beyond the $Cu_2S_2N_2$ core. Although the latter holds the majority of the spin, and, therefore, provides a good approximation for the above calculation of the spin density distribution and the *B* and *C* values, detailed theoretical calculations should eventually account for the larger distribution which may be significant in terms of the electronic properties of the site.

Conclusions

W-band pulsed ENDOR measurements provided symmetric and resolved ^{1}H spectra of the Cu_A centers in N_2OR, M160T9, purpAz, and the M160QT0 mutant. Simulations of orientation selective spectra yielded the A_{iso} values of the four strongly coupled cysteine β-protons. The available 3-D structures show that the H−C−S−S dihedral angles are well conserved. Consequently, the spread of the A_{iso} values of the cysteines' β-protons of a particular Cu_A center provides directly $\rho_S B$ and $\rho_S C$. A negative linear relation was found between the maximum A_{iso} value of the cysteine β-protons and A_{iso}(Cu) (or $A_{||}$(Cu)). This allowed us to refine the relative ρ_S and ρ_{Cu} values of the investigated Cu_A centers, as determined from simulations of the ENDOR spectra using anisotropic hyperfine parameters extracted from the available 3-D structures. Within experimental error, the ENDOR data are consistent with the ρ_S and ρ_{Cu} being similar for the two Cu and S in the Cu_2S_2 core. The largest ρ_S was found for M160T9, and the lowest was found for purpAz. The ρ_S values were further employed to determine the *B* and *C* parameters which give the relative contributions of the hyperconjugation mechanism, manifested by the size of *B*, to the isotropic hyperfine coupling of the cysteine β-protons. Analysis of the ENDOR spectra of the weakly coupled protons showed that the width of their powder patterns at $g_\perp$ is mainly determined by the histidine $H_{\epsilon 1}$ protons and the splitting, often appearing in the outer wings, is a measure of differences in their position with respect to the Cu_2S_2 core. Comparison of the spectral features of M160QT0 with those of the other proteins investigated shows that its Cu_A center is highly symmetric, similar to that in purpAz. Still, it has a smaller spin density on the coppers and smaller $H_{\epsilon 1}$−Cu distances. All proteins show the presence of a proton with a relatively large negative A_{iso} value which is assigned to an amide proton of one of the cysteines.

Acknowledgment. This work has been supported by the German-Israel Foundation for Scientific Research (D.G., I.P., P.M.H.K.). W.G.Z. acknowledges the support of "Fonds der Chemischen Industrie". We thank Dr. Igor Gromov for performing some of the W-band measurements and Stefan Stoll (ETH) for his help regarding the use of his EasySpin toolbox for MatLab (by MathWorks, Inc.).

JA012514J

(60) Slutter, C. S.; Goldfarb D., unpublished results.
(61) Coremans, J. W. A.; Poluektov, O. G.; Groenen, E. J. J.; Canters, G. W.; Nar, H.; Messerschmidt. *J. Am. Chem. Soc.* **1994**, *116*, 3097−3101.
(62) Guzzi, R.; Bizzarri, A. R.; Sportelli, L.; Cannistrato, S. *Biophys. Chem.* **1997**, *63*, 211−219.